The Space Congress® Proceedings

1987 (24th) Space - The Challenge, The Commitment

Apr 1st, 8:00 AM

Design and Development of a Computer Assisted Ground Control Technique for Space Station Robotics

Carl R. Konkel

Phillip E. Harmon Teledyne Brown Engineering Cummings Research Park Huntsville, Alabama

Follow this and additional works at: https://commons.erau.edu/space-congress-proceedings

EMBRY-RIDDLE
Aeronautical University™
SCHOLARLY COMMONS

DESIGN AND DEVELOPMENT OF A COMPUTER-ASSISTED
GROUND CONTROL TECHNIQUE FOR SPACE STATION ROBOTICS

Carl R. Konkel
Phillip E. Harmon
Teledyne Brown Engineering
Cummings Research Park
Huntsville, Alabama

ABSTRACT

Recent design activities for the International Space Station have included studies of the operations and productivity of the U.S. Laboratory module. A major finding was that the most limited resource on the Station will be crew time. A ground-controlled robot has been proposed by Teledyne Brown Engineering that will help alleviate these constraints and allow around-the-clock U.S. Laboratory operations. However, the ground control of a mechanism in Earth orbit imposes command and feedback delays because of the distance and communications network involved. A unique predictive display for use by the ground operator in the presence of varying time delays has been developed and tested and has reduced the "move-and-wait" task times normally associated with delayed feedback teleoperations, minimized operator training, and reduced downlink bandwidth required.

INTRODUCTION

Teledyne Brown Engineering has completed a preliminary design of the equipment necessary to outfit the U.S. Laboratory (USL) module of the International Space Station. This design included the analysis of various user instruments and their operation, both in man-tended and permanently manned configurations. A major finding was that the most limited resource within the USL will be crew time.

Options to improve the situation included deferring experiments or instruments, reducing onboard operations, and increasing crew size or enhancing crew activities using automation and robotic techniques.

It was determined that minimum impact to Space Station resources would occur if a ground-controlled laboratory robot were used to enhance crew activities.

Because of the high potential of this laboratory robot to increase Space Station productivity in the early operational phase of the program, plus the Congressional emphasis on application of robotics, a preliminary design of such an onboard manipulator and the required ground control station was carried out. It was desired to integrate the necessary robotic and teleoperations technologies into a system that would meet the following overall goals:

1) Function safely in a manned environment

2) Operate efficiently in microgravity under nominal and limited off-nominal conditions

3) Provide reasonable accuracy and repeatability

4) Be capable of executing a large percentage of manipulative laboratory tasks

5) Allow ground operators to perform laboratory operations around the clock in the presence of significant time delay

6) Minimize uplink/downlink time and bandwidth.

LABORATORY EXPERIMENT MANIPULATOR SYSTEM

A conceptual design for the onboard portion of a Space Station Laboratory

Experiment Manipulator System (LEMS) is shown in Figure 1. It is a dual-armed unit consisting of modular joints and appendages to a ceiling-mounted track assembly. The track is attached to standard rack hardpoints and is segmented so it can be easily removed in sections if rack access is necessary. The robot concept includes proximity detectors with hardware interrupts and limited force/ torque motors to ensure safe operation in a manned environment.

In an emergency situation, the LEMS can operate in a low-pressure environment for several hours, can be directed to clean up a hazardous spill under onboard or ground control, and can operate under zero visibility. The manipulator interfaces with the Space Station Data Management System (DMS) and Communication and Tracking System (C&TS) for operational control and monitoring. Sufficient speed and memory is provided within the LEMS central processor to allow growth from an initial telerobot to a combined tele-robot/autonomous manipulator.

The goals regarding ground control were met with a Ground Control Station concept, which combines high-speed graphics workstations with digitial imaging processing to form a display and control technique with minimal operator workload. A block diagram of the Ground Control Station is shown in Figure 2. A User Operations Center provides the necessary services to support a dedicated Ground Control Station that can be collocated or remote. The computer-assisted ground control technique will be discussed in detail in the following sections.

TELEROBOTIC FUNCTIONS

It is envisioned that initially most robot manipulative functions would be executed under ground control until sufficient experience and confidence is gained to enable preprogrammed sequences to be built from a "library" of stored commands. This range of manipulative functions should be sized to closely emulate the dexterity and sensitivity of a human. Execution of these functions would then drive the configuration of a Ground Control Station and its displays, hand controls, and other interfaces (such as voice).

Examples of manipulative activities controlled from the ground would be to open a drawer, remove a panel, grasp an object, apply pressure, or turn a knob. These general functions can be divided into capabilities that consist of translation, rotation, manipulation, and environmental sensing. An analysis of human manipulative functions defined in MIL-STD-1472C, NASA Handbook MSFC-HDBK-512A, and Space Station experiment functional flow timelines in the Microgravity and Materials Processing Facility (MMPF) study has resulted in the list shown in Table I.

Functions such as left/right, up/down, and in/out translation can be directly controlled by a wide variety of manually operated transducers, including position or force joysticks with and without lead/ lag compensation. Rotation about three axes can also be controlled by position or force transducers. The recent availability of combined, six degree-of-freedom hand controllers with grip-mounted switches appears promising for laboratory robot control.

Environmental sensing functions shown in Table I include audio, ultrasonic, and visual feedback. Audio and ultrasonic feedback loops would be closed around the onboard manipulator itself to ensure immediate response to object or crew proximity. Until visual processing technology is mature, however, visual feedback will have to be downlinked to the ground control operator, where feedback response will originate. Studies have shown that this visual feedback should consist of at least two orthogonal camera views. Research indicates that stereo vision in most cases has not been necessary in man-in-the-loop tests involving laboratory manipulations similar to peg-in-hole and pick-and-place tasks.

Underlying all these functional requirements for manipulation is the fact that the present and future NASA communications network imposes significant time delays between a ground operator command and the ensuing feedback (video and alphanumeric).

Recent studies of the Tracking and Data Relay Satellite (TDRS) network have shown

that a minimum 3-sec delay will always be present, even for an operator located at the White Sands Missile Range control site. The delay could be as long as 8 sec if all communications satellite, terrestrial relay, and control center delays are taken into account. This significant time delay was determined to be a major challenge for efficient laboratory teleoperations; hence, additional study and a solution were pursued.

GROUND DISPLAYS

The effect of time delay on manipulator control has been analyzed previously, and it was found that the move-and-wait strategy adopted by the test subject resulted in a significant increase in task completion times (up to 40 times in some cases) in direct proportion to task complexity. These results were found applicable to conventional six-degree-of-freedom manipulators, and it was also determined that operator fatigue and the tendency to "drift" while waiting for feedback compounded the problem. Researchers have provided basic computer-generated visual cues within the operator's video display and found them to be useful in the presence of time delay. The Teledyne Brown predictive display takes the next step and provides a full robot simulation overlay to guide the operator.

It was decided that a high-speed graphics workstation would be necessary to simulate both live, delayed video from a laboratory robot and a predicted robot image based on a high-fidelity kinematic, dynamic, and control model. A photograph of an initial configuration is shown in Figure 3. Since an operator would use a controller device to maneuver the robot, it was required that the animation be as smooth and realistic as possible. This resulted in choosing a computer with Z-plane buffering and 60-Hz noninterlaced display for the simulation.

The approach used in the predictive display required: 1) the execution in real time of the robot motion equations governing kinematics, dynamics, and control and 2) an animated visual image corresponding to all or part of the physical robot. A block diagram of the basic robot motion model is shown in Figure 4. The feasibility of doing both model and animation computations in real time was first analyzed, and the results for the robot model motion equations are shown in Table II.

The first two columns of values represent the number of multiplications and additions required to execute the corresponding relations for calculating robot inverse kinematics, coupled/uncoupled dynamics, and control. For this case, a standard proportional + integral + derivative (PID) control algorithm was assumed. The resultant execution times shown in the third column are the approximate times in milliseconds for the equation to be calculated using a 68020 microprocessor operating at 16 MHz. The data indicates that a total of approximately 4 msec per execution cycle is required to calculate robot model response.

The processing power required for animation computations was next estimated. The graphics performance of a typical 32-bit workstation can be quantified in terms of point transformations per second. Using 110,000 floating point coordinates per second as a typical benchmark, a shaded, solid polygon representing a robot image consisting of 500 points can be translated, rotated, and scaled every 5 msec.

It is, therefore, concluded that the total robot model execution time will be on the order of 9 msec. This is compatible with the desired execution rate of 25 Hz (40 msec per cycle).

ROBOT MODEL DEVELOPMENT

In developing the equations of motion for a typical robot arm, the first step was to set up the appropriate coordinate system at each joint and at the base. The most common convention is that of Paul and is to place the coordinate frame at the end of its respective link. All the consecutive reference frames would have a common post-rotated directed for the X-axis. The Z-axis would be in the direction motion of the next link, as shown in Figure 5. The generalized transformation equation for A_n and the

expanded 4x4 homogeneous matrix form for A_n and specific axes, A_1, A_3, and A_4, are also shown in Figure 5.

Table III describes the translation and rotation required to perform the coordinate transformation between the base and the end effector using the standard notation convention from Paul. The A_1, A_3, and A_4 matrices and their inverse forms are calculated by (1), (2) and (3) as follows:

$$(1) \quad A_1 = \begin{bmatrix} c_1 & 0 & s_1 & 0 \\ s_1 & 0 & -c_1 & 0 \\ 0 & 1 & 0 & 0 \\ 0 & 0 & 0 & 1 \end{bmatrix}$$

$$A_1^{-1} = A_1^T = \begin{bmatrix} c_1 & s_1 & 0 & 0 \\ 0 & 0 & 1 & 0 \\ s_1 & -c_1 & 0 & 0 \\ 0 & 0 & 0 & 1 \end{bmatrix}$$

$$(2) \quad A_3 = \begin{bmatrix} c_3 & -s_3 & 0 & -a_3 s_3 \\ s_3 & c_3 & 0 & a_3 c_3 \\ 0 & 0 & 1 & 0 \\ 0 & 0 & 0 & 1 \end{bmatrix}$$

$$A_3^{-1} = \begin{bmatrix} c_3 & s_3 & 0 & 0 \\ -s_3 & c_3 & 0 & 0 \\ 0 & 0 & 1 & 0 \\ -a_3 s_3 & a_3 c_3 & 0 & 1 \end{bmatrix}$$

$$(3) \quad A_4 = \begin{bmatrix} c_4 & -s_4 & 0 & -a_4 s_4 \\ s_4 & c_4 & 0 & a_4 c_4 \\ 0 & 0 & 1 & 0 \\ 0 & 0 & 0 & 1 \end{bmatrix}$$

$$A_4^{-1} = \begin{bmatrix} c_4 & s_4 & 0 & 0 \\ -s_4 & c_4 & 0 & 0 \\ 0 & 0 & 1 & 0 \\ a_4 s_4 & a_4 c_4 & 0 & 1 \end{bmatrix}$$

where

$c_n = \cos \theta_n$
$s_n = \sin \theta_n$
$a_n = \text{link length}_n.$

The resultant transformation matrix T_4 is calculated by (4),

$$(4) \quad T_4 = A_1 A_3 A_4.$$

Using the additive trigonometric identities, T_4 can be calculated, yielding (5):

$$(5) \quad T_4 = \begin{bmatrix} n_x & o_x & a_x & p_x \\ n_y & o_y & a_y & p_y \\ n_z & o_z & a_z & p_z \\ 0 & 0 & 0 & 1 \end{bmatrix}$$

where

$p_x = c_1 (-a_4(s_3 c_4 + c_3 s_4) - a_3 s_3)$
$p_y = s_1 (-a_4(s_3 c_4 + c_3 s_4) - a_3 s_3)$
$p_z = a_4 (c_3 c_4 - s_3 c_4) + a_3 c_3.$

The matrix entries n, o, and a for each axis are of similar form and are not shown here.

The inverse kinematic relations can then be derived for each joint angle. The first joint angle is derived using $A^{-1}T_4 = A_3 A_4$, and equating the row 3, column 4 element of each resultant concatenated matrix yields:

$$(6) \quad \theta_1 = \tan^{-1} (p_y)/(p_x).$$

The second joint angle is derived as a function of p_x, p_y, p_z, w, and v, as follows:

By equating elements (1,4) and (2,4) of $A_1^{-1}T_4$ and $A_3 A_4$, the following two equations are obtained.:

(6) $c_1 p_x + s_1 p_y = -c_3 a_4 s_4 - s_3(a_4 c_4 + a_3)$

(7) $p_z = -s_3 a_4 s_4 + c_3(a_4 c_4 + a_3)$.

Squaring and summing these two equations yields:

$$c_4 = \frac{(c_1 p_x + s_1 p_y)^2 + p_z^2 - (a_4^2 + a_3^2)}{2 a_3 a_4} .$$

Using the identity

$$s_4 = \sqrt{1 - c_4^2}$$

results in:

$$\theta_4 = \tan^{-1}(s_4/c_4).$$

Solving for c_3 and s_3 simultaneously from (6) and (7) and letting

$$v = a_4 s_4$$

$$w = a_4 c_4 + a_3$$

results in:

$$\theta_3 = \tan^{-1}(s_3/c_3) .$$

where $s_3 = \dfrac{w(c_1 p_x + s_1 p_y) + v p_z}{-(v^2 + w^2)}$

$$c_3 = \frac{v(c_1 p_x + s_1 p_y) - w p_z}{-(v^2 + w^2)} .$$

SIMULATION DESCRIPTION

The kinematic equations described above were used to simulate the real robot image and the predicted robot image. Figure 6 is a photograph of the computer display, showing the simulated live video as a shaded solid and the robot model or "phantom" in solid white. In the background is a representation of the laboratory module, including racks mounted in the walls and cameras mounted in the bulkheads. Additional views from the ceiling-mounted carriage and the end effector are available. At any time, the operator may call up a different view and zoom, pan, and tilt the simulated camera. Execution speed is rapid enough so all motion appears realistic.

Initial tests were carried out using a three-button mouse, keypad, and color display. Either individual joint control or resolved XYZ position control modes may be chosen. As shown in the flow diagram of Figure 7, robot position data is sent to the simulation, which calculates the motion required based on the derived kinematic equations. Motion commands update the location and position of the "phantom" arm in operator real time. A motion data stack within the computer receives the motion commands and saves them for execution by the simulated onboard robot. Selectable delays between 3 and 8 sec are available.

WORK IN PROCESS

Currently being tested is a predictive display combining live video with computer imagery on a single display. A "digital rotoscope" technique is being used to overlay the live video with a computer-generated robot image. The white "phantom" image responds immediately to operator commands so that immediate feedback is sensed, while live video from the orbiting station is actually delayed 3 to 8 sec. Findings to date include the following:

1) Operator familiarity is almost immediate and the phantom is soon used exclusively.

2) Retraining under different time delays is minimized because the operator uses an image with fixed (equal to zero) delay.

3) Users can practice a motion using the phantom prior to on-line execution (uplink).

4) Low-frame-rate video from the station can be used to conserve bandwidth and thereby increase teleoperations opportunities.

A test of this ground control technique with an actual flight manipulator has been proposed to NASA as a part of the inspace technology development experiment program. The proposed system consists of a modified, industrial-type robot mounted to a vertical rack within a Spacelab module on a Space Shuttle mission. Figure 8

illustrates the physical arrangement using an Intelledex anthropomorphic manipulator. Two adjacent task panels are used to test robot dynamics in microgravity and to allow the performance of typical laboratory tasks. A ground control console based on the simulation work done to date is envisioned to enable man-in-the-loop operations to be carried out using the existing NASA Payload Operations Control Center (POCC) plus application software for direct ground control.

REFERENCE

Paul, R. P., *Robot Manipulators: Mathematics, Programming & Control.* MIT Press, Cambridge, MA 1981.
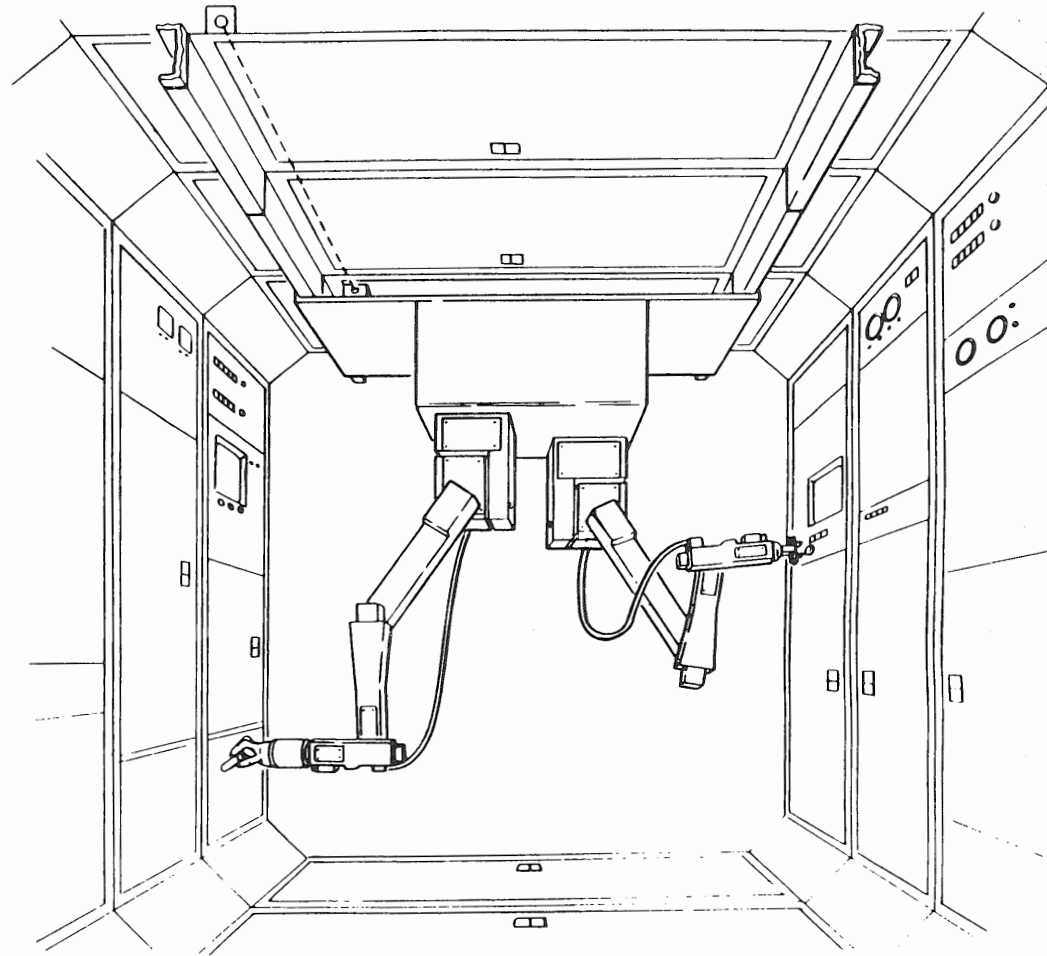
FIGURE 1. CONCEPTUAL DESIGN FOR SPACE STATION LABORATORY
EXPERIMENT MANIPULATOR SYSTEM (LEMS)

VIDEO/COMM ARCHIVE

OFF-LINE PROCESSING SYSTEM

NEAR REAL TIME

JOYSTICK

DISK AND 1/4" TAPE CONTROLLER

170 MB DISK

CARTRIDGE TAPE

OPTIONAL FLOATING POINT ACCELERATOR

68020 PROCESSOR

FRAME BUFFER CONTROLLER
GEOMETRY ENGINES

UPDATE CONTROLLER

DISPLAY CONTROLLER | COLOR MAP

RGB TO MONITOR

MEMORY

DISPLAY MEMORY (1024 ^{2} X 4)

KU BAND
VIDEO
S-BAND
A/G VOICE
VOICE
MCC DATA
CMD
MIPS

N A S A   C O M M

DATA ACQUISTION, DISTRIBUTION AND PLAYBACK

HRS CONTROL
OD
MCC DATA
CMD'S
HIGH RATE

DATA PROCESSING

STATUS PARAMETERS
OD PARAMETERS
MCC DATA
COMMANDS
USER DATA

TERMINAL

VIDEO DIGITIZER
FRAME BUFFER
REAL TIME CONVOLVER
PIPELINE PROCESSOR

CONVERTER

GROUND CONTROL STATION

CMD

S T A N D A R D   I N T E R F A C E

COMMANDS
DIGITAL DATA

ANALOG / VIDEO
HIGH RATE CHANNELS

COMMANDS

VIDEO

CONVERTER

TBE-858-87/2-25

TBE-859-87/2-25

USER OPERATIONS CENTER

FIGURE 2. GROUND CONTROL STATION AND USER OPERATIONS CENTER INTERFACE FOR SPACE STATION LABORATORY TELEOPERATIONS
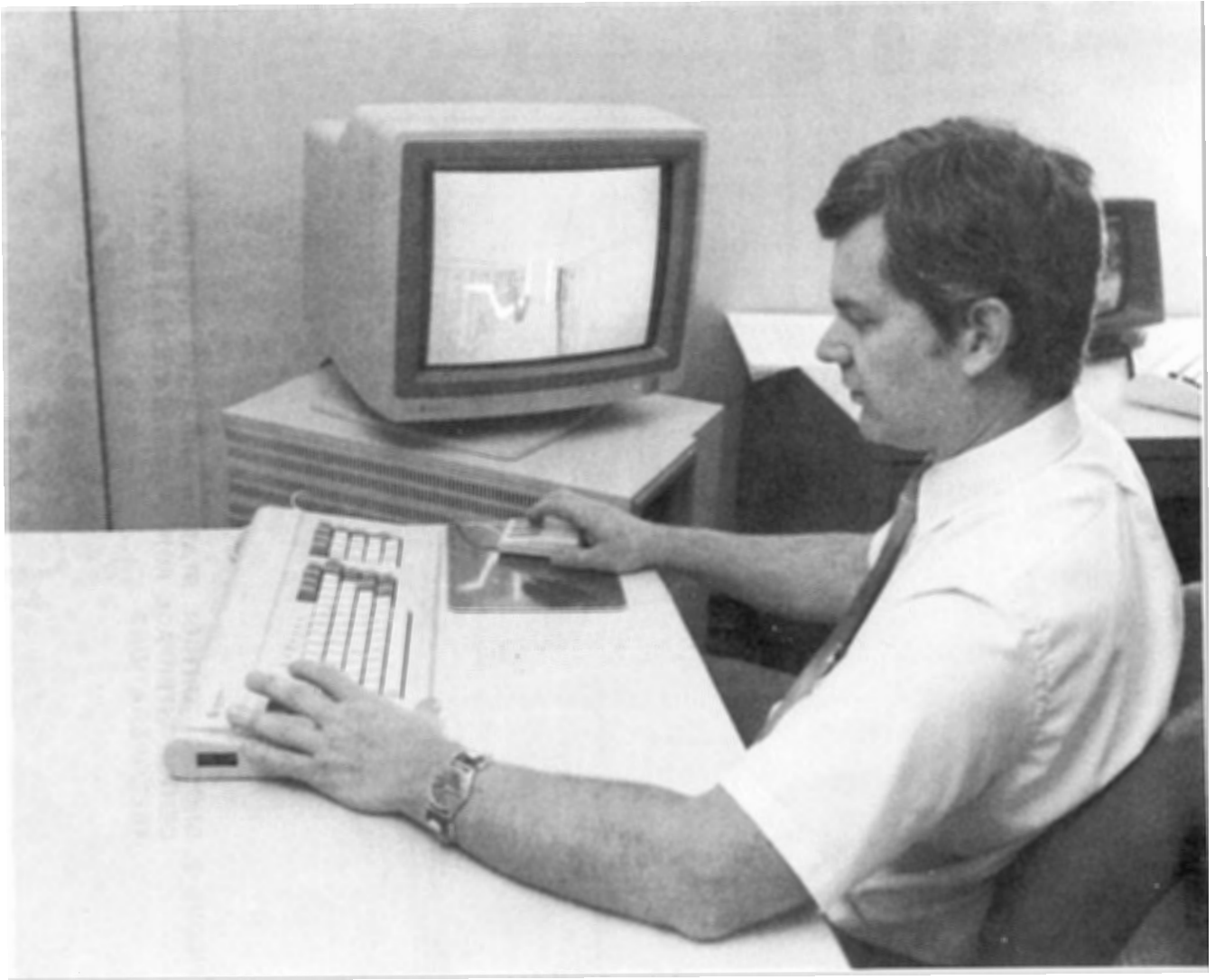
FIGURE 3. TELEROBOTIC GROUND CONTROL STATION SIMULATION WITH PREDICTIVE DISPLAY

KINEMATICS   CONTROL   DYNAMICS

Λ^{-1} : INVERSE KINEMATICS TRANSFORMATIONS

$M(\Theta)$: MASS MATRIX

$\tau_{V(\theta,\dot\theta)}$: TORQUE DUE TO VELOCITY EFFECTS (CENTRI FUGAL, CORIOLIS)

$\tau_{f(\theta,\dot\theta,F)}$: TORQUE DUE TO FRICTION

F: FORCE

G(z): SERVO TRANSFER FUNCTION

K_D : GAIN FOR DERIVATIVE COMPONENT

K P: GAIN FOR PROPORTIONAL COMPONENT

K_I : GAIN FOR INTEGRAL COMPONENT
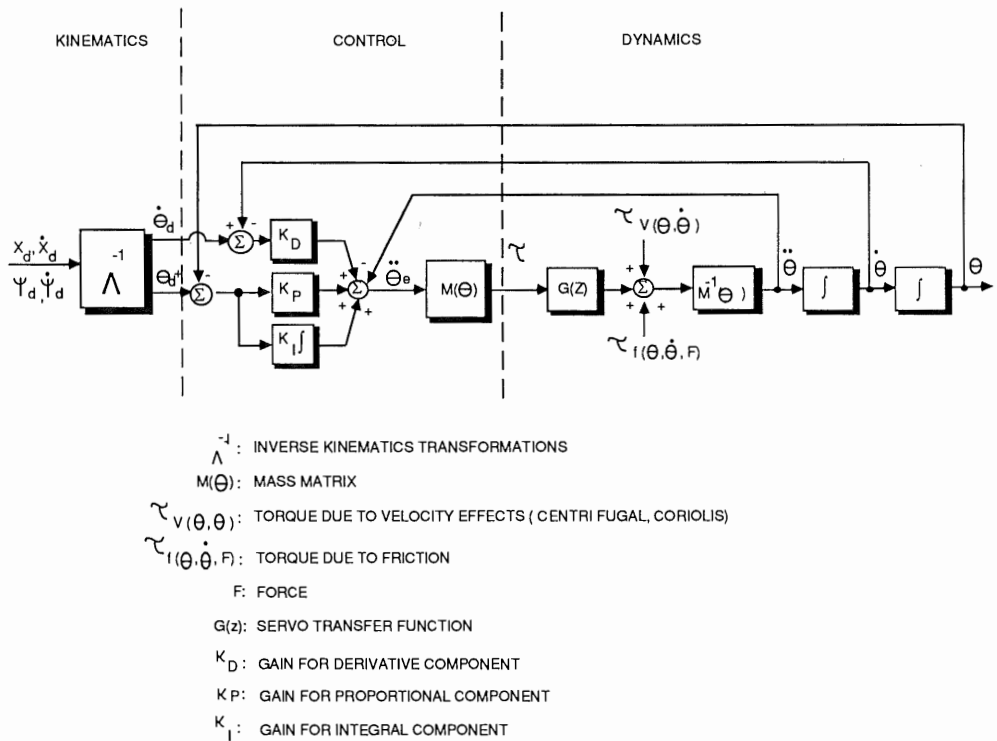
TBE-842-86/11-19

FIGURE 4. ROBOT MOTION MODEL WITH KINEMATIC/
DYNAMIC/CONTROL ALGORITHMS

FIGURE 5. ROBOT KINEMATIC MODEL
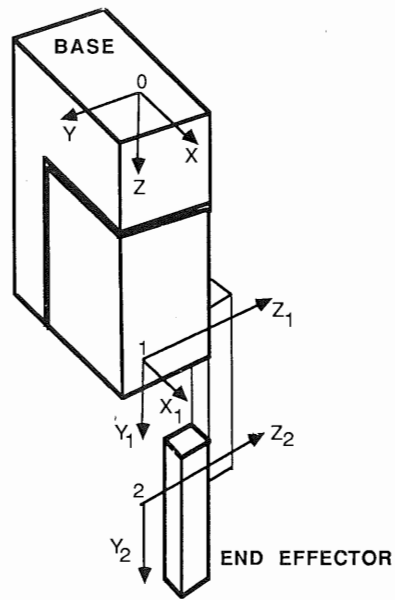
$$An = Rot(z, \theta) \; Trans(0,a,0) \; Rot(x, \alpha)$$

$$An = \begin{bmatrix} C_\theta & -S_\theta & 0 & 0 \\ S_\theta & C_\theta & 0 & 0 \\ 0 & 0 & 1 & 0 \\ 0 & 0 & 0 & 1 \end{bmatrix} \begin{bmatrix} 1 & 0 & 0 & 0 \\ 0 & 1 & 0 & a \\ 0 & 0 & 1 & 0 \\ 0 & 0 & 0 & 1 \end{bmatrix} \begin{bmatrix} 1 & 0 & 0 & 0 \\ 0 & C_\alpha & -S_\alpha & 0 \\ 0 & S_\alpha & C_\alpha & 0 \\ 0 & 0 & 0 & 1 \end{bmatrix}$$

$$An = \begin{bmatrix} C_\theta & -S_\theta C_\alpha & S_\theta S_\alpha & -aS_\theta \\ S_\theta & C_\theta C_\alpha & -C_\theta S_\alpha & aC_\theta \\ 0 & S_\alpha & C_\alpha & 0 \\ 0 & 0 & 0 & 1 \end{bmatrix}$$

$$A_1 = Rot(z, \theta_1) \; Rot(X, \alpha)$$

$$A_3 = Rot(Z, \theta_3) \; Trans(o, a_3, 0)$$

$$A_4 = Rot(z, \theta_4) \; Trans(0, a_4, 0)$$
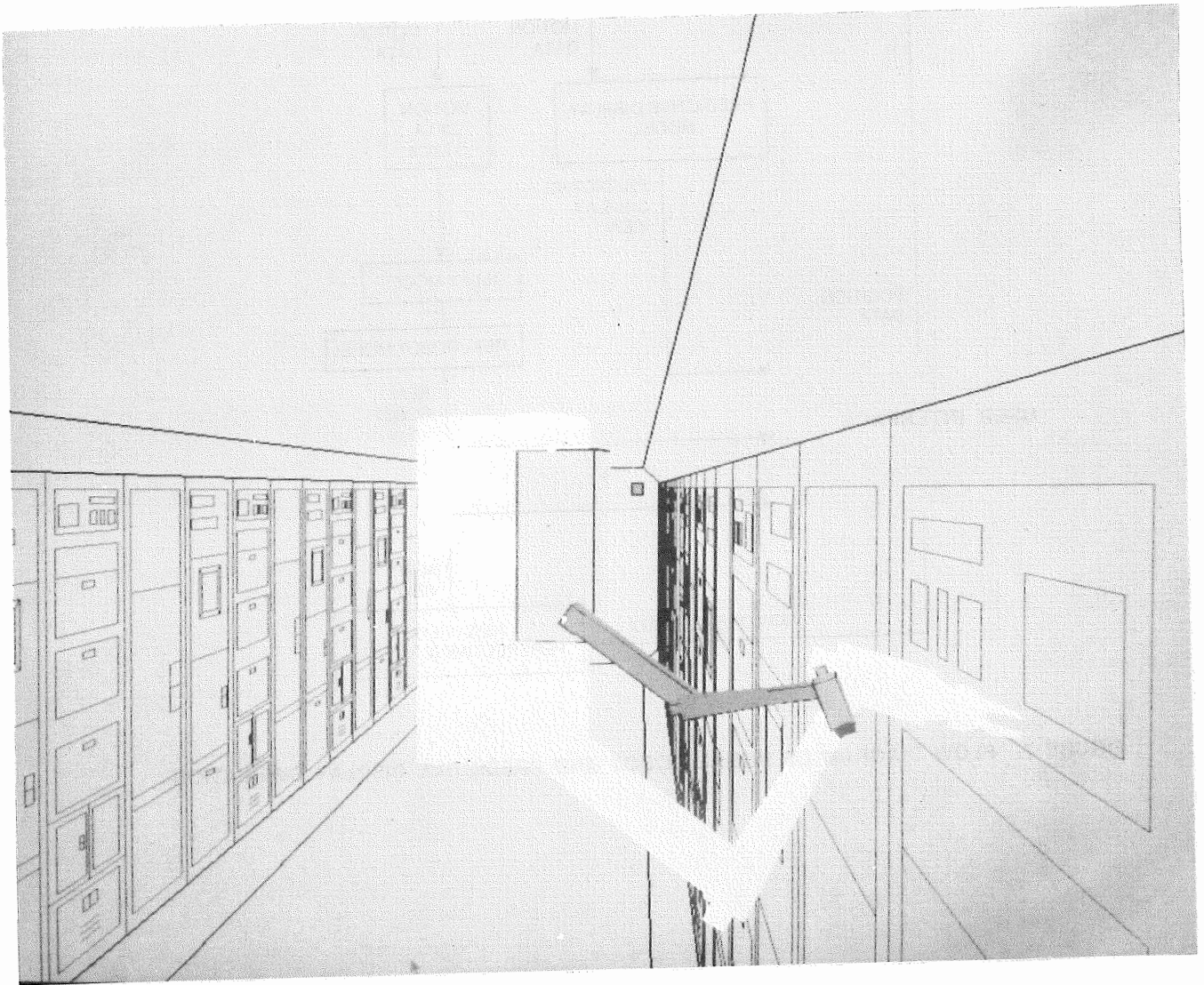
FIGURE 6. TELEDYNE BROWN PREDICTIVE DISPLAY SIMULATION
FOR SPACE STATION TELEROBOTICS
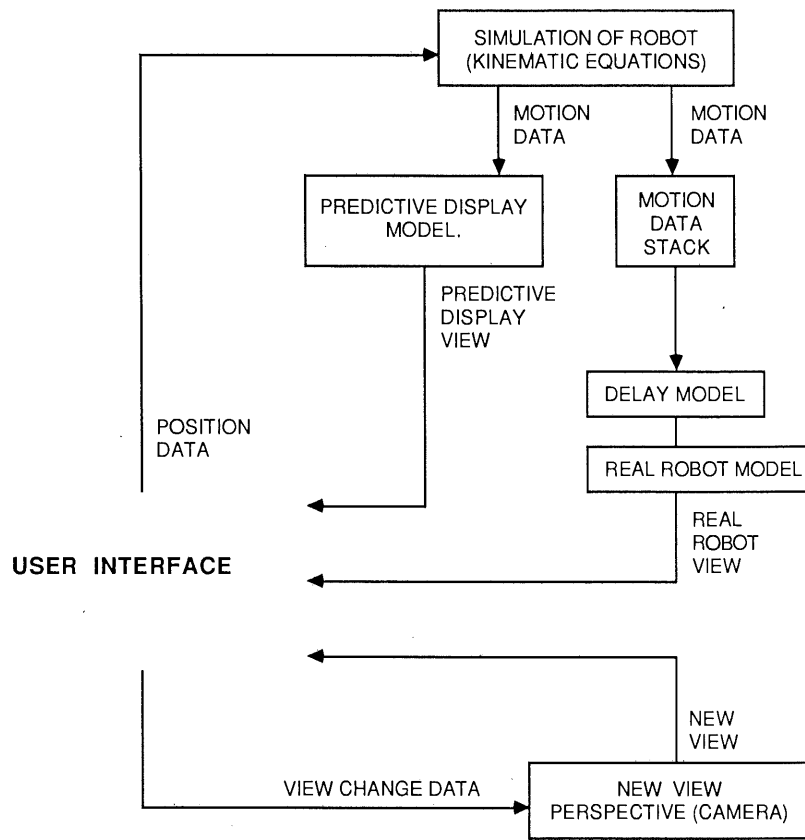
FIGURE 7. FLOW DIAGRAM OF INITIAL ROBOT AND PREDICTIVE DISPLAY SIMULATION

STANDARD SPACELAB
SINGLE RACK

TASK PANEL

TLEM

TASK PANEL
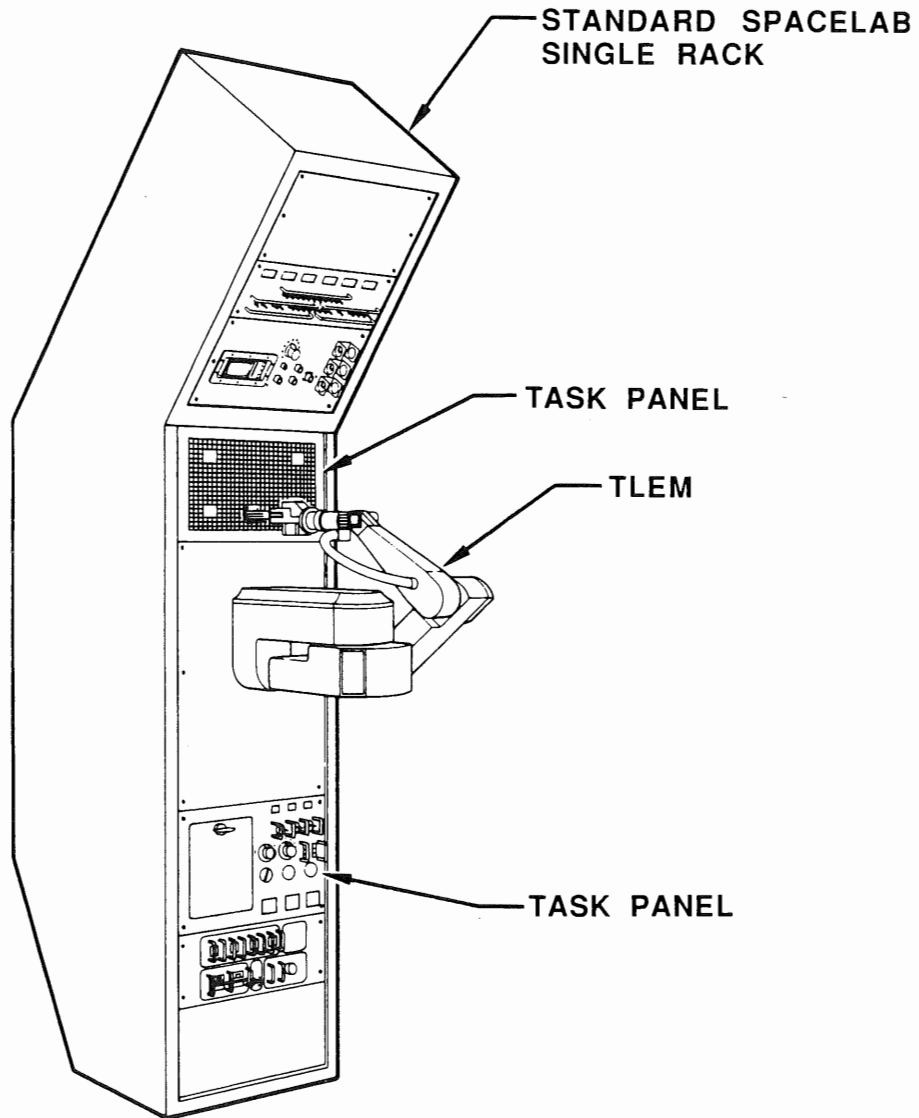
FIGURE 8. PROPOSED SPACE SHUTTLE TELEOPERATED
FLIGHT EXPERIMENT

TABLE I. SPECIFICATION OF MANIPULATIVE FUNCTIONS FOR SPACE STATION LABORATORY ROBOT

CATEGORY	FUNCTION	SPECIFICATION	MAXIMUM	MINIMUM
TRANSLATION	LEFT / RIGHT	DISTANCE MASS SIZE FORCE	11.8 M(38.7ft) 30 kg (66 ib) 0.23x0.33x0.4m(9x13x16in) 98 N(22 lbf)	2 mm (0.08 in) 0.004 kg (0.009 lb) 1.1x3.8x0.025 cm (0.4x1.5x0.01in) 3 N(0.6 lbf)
	UP/DOWN	DISTANCE MASS SIZE FORCE	231 cm (84 in) 2.25 kg (5 lb) 30.5x5x5 cm (12x2x2 in) 116 N(22 lbf)	2 mm (0.08 in) 0.0045 kg (0.01 lb) 3 N (0.6 lbf)
	IN/OUT	DISTANCE MASS SIZE FORCE	5 cm (2 in) 2.25 kg (5 lb) 2.5 cm (1 in) 249 N(56 lbf)	0.2 cm (0.078 in) 0.0045 kg(0.01 lb) 0.6 cm (0.25 in) 1.4 N(0.3 lbf)
		ACCURACY REPEATABILITY		5 mm (0.2 in) 1 mm (0.04 in)
ROTATION	CW/CCW	INCREMENT RATE EXCURSION TORQUE	1 degree 180 degree/sec 340 degrees 20 N-m (14.75 lb-ft)	0.1 degree 1 degree/sec 3.8 N-m (2.8 lb-ft)
		ACCURACY REPEATABILITY		0.1 degree 0.02 degree
MANIPULATION	GRAB / HOLD / RELEASE	DISPLACEMENT MASS SIZE FORCE	7.5 cm (3 in) 2.25 kg (5 lb) 10 cm (4 in) 260 N (59 lbf)	0 0.0045 kg (0.01 lb) 0.32 cm (0.3 lbf) 1.4 N (0.3 lbf)
	CONTACT	SENSITIVITY	10 N (2.2 lb)	0.01 N (0.0022lb)
	USE	TRACKING FREQUENCY DAMPING RATIO		1 Hz 0.7
ENVIRONMENTAL	ULTRASONIC DETECTION	CONFIGURATION RANGE RESOLUTION	 1.5 M (5 ft)	COMBINED TRANSMITTER / RECEIVER 0.3 m(1 ft) 0.3 cm (0.12 in)
	INFRARED DETECTION	CONFIGURATION RANGE RESOLUTION	 1.5 M (5 ft)	FOCUSED RECEIVER 0.3m (1 ft) 7.5 degrees
	VISUAL	CONFIGURATION RANGE RESOLUTION FRAME RATE GRADATION SENSITIVITY	 2.5 cm (1 in) 30	TWO ORTHOGONAL CAMERAS 12.2 m (40 ft) 0.025 cm (0.01 in) 1 256 30 lux (3 ft-c)
	AUDIO	CONFIGURATION RANGE RESOLUTION (INPUT)		VOICE OUTPUT / TONE OUTPUT VOICE INPUT 12.2 m (40 ft) 100 words, speaker independent

TBE-1124-86/12-2

TABLE II. ESTIMATE OF SIMULATION EXECUTION TIME FOR ROBOT MODEL MOTION EQUATIONS

	MULT	ADD	EXECUTION TIME (MILLISEC)
INVERSE KINEMATICS			
Joint Angles	25	10	0.10
Joint Velocities	216	125	1.02
Joint Accelerations	---	---	---
DYNAMICS			
Uncoupled/Idealized	200	150	1.16
Coupled/Idealized	270	230	1.48
Coupled/Nonlinear	350	300	1.92
CONTROL			
PID	25	10	0.10
Mass Matrix (without load)	12	10	0.06
Mass Matrix (with varying load)	27	17	0.13

Kinematics:

(Position) $[X]_n = A_1(\theta) A_2(\theta) \cdots A_{n-1}(\theta) A_n(\theta) [X]_o$

where $[X]_n$ = position vector of end effector

$[X]_o$ = position vector of base

A_n = transformation matrix for link n

θ = joint angle vector

(Velocity) $[\dot{X}\,\dot{Y}\,\dot{Z}\,\dot{\theta}\,\dot{\psi}\,\dot{\phi}]^T = J(\theta)\,[\dot{\psi}_1\,\dot{\theta}_1\,\dot{\theta}_2\,\dot{\theta}_3\,\dot{\psi}_3\,\dot{\psi}_2]^T$

where $[\dot{X}\,\dot{Y}\,\dot{Z}\,\dot{\theta}\,\dot{\psi}\,\dot{\phi}]$ = 6-DOF end effector vector

$[\dot{\psi}_1\,\dot{\theta}_1\,\dot{\theta}_2\,\dot{\theta}_3\,\dot{\psi}_3\,\dot{\psi}_2]$ = 6-DOF joint vector

$= J(\theta)$ = Jacobian matrix

Dynamics: $\tau = M(\theta)\,\ddot{\theta} + V(\theta,\dot{\theta}) + f(\theta,\dot{\theta},F)$

where $M(\theta)$ = mass matrix of manipulator

$V(\theta,\dot{\theta})$ = velocity effect vector
(centrifugal/coriolis)
(gravity effect = 0)

$f(\theta,\dot{\theta},F)$ = friction effect vector

τ = joint torque vector

Control: $\tau = M(\theta)\,[K_D(\dot{\theta}_d - \dot{\theta}) + K_p(\theta_d - \theta) + K_I \int (\theta_d - \theta)\,d_\tau - \ddot{\theta}\,] + NL$

where K_D = derivative gain

K_p = proportional gain

K_I = integral gain

NL = nonlinear terms = $\tau_{V(\theta,\dot{\theta})} + \tau_{f(\theta,\dot{\theta},F)}$

LINK	VARIABLE	α	a	d	$C\alpha$	$S\alpha$
1	θ_1	a_0	0	0	0	1
3	θ_3	0	a_3	0	1	0
4	θ_4	0	a_4	0	1	0

**TABLE III. NOTATION CONVENTION FOR COORDINATE
TRANSFORMATION MATRICES**

TBE-866-87/2-27